

Article

# Signal Enhancement of Helicopter Rotor Aerodynamic Noise Based on Cyclic Wiener Filtering

Chengfeng Wu <sup>1,2</sup>, Chunhua Wei <sup>2,\*</sup>, Yong Wang <sup>2</sup>  and Yang Gao <sup>1</sup> 

<sup>1</sup> School of Information Engineering, Southwest University of Science and Technology, Mianyang 621010, China; wcf302751794@126.com (C.W.); gaoyang@caep.cn (Y.G.)

<sup>2</sup> State Key Laboratory of Aerodynamics, China Aerodynamics Research and Development Center, Mianyang 621000, China; wangyong@cardc.cn

\* Correspondence: wch410204603@126.com

**Abstract:** The research on helicopter rotor aerodynamic noise becomes imperative with the wide use of helicopters in civilian fields. In this study, a signal enhancement method based on cyclic Wiener filtering was proposed given the cyclostationarity of rotor aerodynamic noise. The noise was adaptively filtered out by performing a group of frequency shifts on the input signal. According to the characteristics of rotor aerodynamic noise, a detection function was constructed to realize the long-distance detection of helicopters. The flight data of the Robinson R44 helicopter was obtained through the field flight experiment and employed as the research object for analysis. The detection range of the Robinson R44 helicopter after cyclic Wiener filtering was increased from 4.114 km to 17.75 km, verifying the feasibility and effectiveness of the proposed method. The efficacy of the proposed detection method was demonstrated and compared in the far-field flight test measurements of the Robinson R44 helicopter.

**Keywords:** rotor; aerodynamic noise; cyclic Wiener filtering; long-distance detection



**Citation:** Wu, C.; Wei, C.; Wang, Y.; Gao, Y. Signal Enhancement of Helicopter Rotor Aerodynamic Noise Based on Cyclic Wiener Filtering. *Appl. Sci.* **2022**, *12*, 6632. <https://doi.org/10.3390/app12136632>

Academic Editor: Subhas Mukhopadhyay

Received: 23 May 2022

Accepted: 27 June 2022

Published: 30 June 2022

**Publisher's Note:** MDPI stays neutral with regard to jurisdictional claims in published maps and institutional affiliations.



**Copyright:** © 2022 by the authors. Licensee MDPI, Basel, Switzerland. This article is an open access article distributed under the terms and conditions of the Creative Commons Attribution (CC BY) license (<https://creativecommons.org/licenses/by/4.0/>).

## 1. Introduction

The noise problem has become an important factor affecting the lives of residents. Erickson examined the effects of background noise on infants and children [1]. Minichilli investigated the impact of background noise on school students aged between 11 and 18 years, and their level of annoyance was often related to background noise [2]. Rossi analyzed the effect of low-frequency noise on cognitive performance of young people aged 19 to 29 years, based on changes in their heart rates [3]. Petri studied the effects of exposure to road, railway, airport, and recreational noise on blood pressure and hypertension, especially for people aged 37 to 72 years [4]. Furthermore, literature [5] investigated seafarers' cognition and attitude towards ship noise emission and raised seafarers' perceptions of the impact of noise on their health. In addition, if the background noise is too strong, the target signal will be overwhelmed, affecting our ability to obtain information. When the background noise is too strong, on the one hand, it affects the health of the listener, on the other hand, in order to obtain the target signal more effectively, some methods need to be used to filter the background noise. During the flight of the helicopter, there is a strong background noise, which will limit the detection distance of the helicopter. Therefore, in order to achieve helicopter detection at a longer distance, it is necessary to filter the background noise.

Helicopters, as an air transport platform, usually make full use of terrain and other conditions to fly at low or ultra-low altitudes when performing rescue missions. They have the advantage of being difficult to be detected by radar, infrared, and other detection methods. The helicopter adopts the rotor to provide lift, propulsion, and control force, with a unique vertical take-off and landing, as well as hovering, high maneuverability, and low-altitude and low-speed flight performance [6]. However, the rotor generates strong

medium- and low-frequency noise, the attenuation in the air is slow, and the propagation distance is long [7–9]. The rotor aerodynamic noise presents time-varying, non-stationary, and multi-harmonic characteristics under the influence of various conditions such as the atmosphere, mountainous environments, fuselage scattering, and flight state when the helicopter is flying in complex environments, such as mountainous areas [10]. Therefore, the investigations of helicopter rotor aerodynamic noise have become a crucial topic of research nowadays.

Helicopter flight noise is mainly derived from the main rotor, tail rotor, and engine. Among them, the former two belong to rotor noise, and the latter is non-rotor noise. The engine noise is related to the high-frequency part and attenuates rapidly in the air. Meanwhile, the noise reduction of the engine can be achieved through the engine design. The aerodynamic noise of the main and tail rotor is mainly in low frequency and slowly attenuates in the air; it is the focus of helicopter noise research [11]. The SNR (signal-to-noise ratio) is extremely low when the helicopter noise signal is received over long distances due to attenuation, since it propagates through the atmosphere. However, the frequency component of rotor aerodynamic noise is low and propagates far in the air during the long-distance detection of the helicopter. Hence, it is the key to helicopter detection.

According to the different generation mechanisms and propagation directions of various noises, helicopter rotor aerodynamic noise can be divided into thickness noise, loading noise, blade vortex interaction (BVI) noise, high-speed impulse (HSI) noise, and broadband noise [8,9]. Thickness noise and loading noise are also commonly referred to as rotation noise [7]. The rotation process of the blade aerodynamic force and the rise of the air volume pulsation constitute the low frequency part of the rotor noise. BVI noise is generated due to the mutual interference between the aerodynamic characteristics of the blades and the vortex shedding from the tip of the propeller. HSI noise usually refers to a kind of impulse noise caused by the surge wave when the helicopter flies forward at a high speed [12]. Turbulence near the blade surface creates broadband noise [13].

A cyclostationary signal is a kind of special non-stationary signal with hidden periodicity. The cyclostationarity signal is a powerful tool for processing random signals with hidden periodic phenomena. Cyclostationary signal processing methods are used in various fields such as bearing fault diagnosis and mechanical source separation [14–21]. However, there is little research on its application to the aerodynamic noise of helicopter rotors. Few people might have linked rotor aerodynamic noise to cyclostationarity before. While the helicopter is flying and hovering, the rotor aerodynamic noise has the characteristics of cyclostationarity ascribed to the periodic movement of the rotor [22,23]. Therefore, the application of cyclostationary analysis methods in aeroacoustics has gradually received extensive attention [19–25]. Antoni, as a top scholar in the field of cyclostationary signals, proposed a variety of methods to extract cyclostationary signals [24], and gradually applied them to the field of aeroacoustics [25]. However, compared with reference [25], the cyclic Wiener filter only needs one microphone to extract the acoustic signal, and the implementation of this method is simpler. Reference [26] gives a method for detecting helicopters by radar, but helicopters are not easy to detect by radar when helicopters fly at an ultra-low altitude. However, we use acoustic signals to detect the helicopter in this paper, because there must be a noise signal when the helicopter is flying. Yu et al. proved the cyclostationarity of rotor aerodynamic noise [22] and proposed a cyclostationary modeling method of helicopter rotor aerodynamic noise [23].

The cyclic Wiener filter can effectively extract the signal with cyclostationarity from the noise signal without cyclostationarity [27–29]. Therefore, this method has a significant enhancement effect on the rotor aerodynamic noise signal with cyclostationary characteristics. Envelope spectrum analysis based on the Hilbert transform is effective in extracting feature frequency, and it is frequently applied in bearing fault diagnosis [30]. However, the characteristic frequencies of bearing faults are generally cyclostationary [31,32]. Therefore, it can be adopted for rotor aerodynamic noise spectrum analysis.

The innovations and main contributions of this paper are described as follows:

1. Aiming at the cyclostationary characteristics of helicopter rotor aerodynamic noise, a cyclic Wiener filter is proposed to be used in the field of helicopter rotor aerodynamic noise enhancement.
2. The cyclic frequency of helicopter rotor aerodynamic noise at different distances is obtained by the cyclostationary analysis method, and it is used for frequency shifting in cyclic Wiener filtering.
3. It is proposed to use the envelope spectrum based on the Hilbert transform to analyze the effect before and after filtering, because the envelope spectrum can eliminate some unnecessary frequency interference and highlight the rotor aerodynamic noise signal with cyclostationarity.
4. According to the harmonic characteristics of helicopter rotor aerodynamic noise, a simple and practical detection method is constructed and combined with cyclic Wiener filtering, which can greatly improve the detection distance of helicopters.

In this paper, a cyclic Wiener filter was constructed and used for the enhancement of helicopter rotor aerodynamic noise, and the filtering effect was analyzed through the envelope spectrum. Furthermore, a detection function was constructed under the consideration of the characteristics of rotor aerodynamic noise, so as to realize the long-distance detection of helicopters. In Section 2, the related theories and methods of cyclic Wiener filtering were introduced in detail, as well as how to realize the filtering of rotor aerodynamic noise. In Section 3, why the envelope spectrum was used for analysis and how to obtain the envelope spectrum through the Hilbert transform were explained. Afterward, through the experiment, the cyclic Wiener filter was completed, and the long-distance detection of the helicopter was realized in Section 4. Finally, conclusions were drawn in Section 5.

## 2. Theory

The operation of rotating machines determines that any type of rotating machine can be modeled with cyclostationary. Antoni summarized the research on the cyclostationary mechanism of various rotating machines [14–17]. Given the periodic motion of the rotor when the helicopter is flying and hovering, the aerodynamic noise of the rotor presents cyclostationarity. However, ambient noise can be filtered out by the cyclic Wiener filter since it is not cyclostationary.

### 2.1. Spectral Coherence Theory

Antoni obtained the cyclic spectral coherence theory [15–17] when he studied the analysis method of cyclostationary signals. The time average correlation coefficient  $\rho_x^\alpha(f)$  of signal  $x(t)$  at  $f - \alpha/2$  and  $f + \alpha/2$  is called spectral correlation function, defined as

$$\rho_x^\alpha(f) = \frac{S_x^\alpha(f)}{[\langle S_x \rangle(f + \alpha/2) \langle S_x \rangle(f - \alpha/2)]^{1/2}} \tag{1}$$

where  $\rho_x^\alpha(f)$  denotes the Fourier transform of the cyclostationary autocorrelation function,  $S_x^\alpha(f)$ , of the signal,  $x(t)$ , with respect to the time delay,  $\tau$ , called the cyclic spectral correlation density function:

$$S_x^\alpha(f) = \int_{-\infty}^{\infty} R_x^\alpha(\tau) e^{-j2\pi f\tau} d\tau \tag{2}$$

$\langle \cdot \rangle$  represents the time average factor:

$$\langle \cdot \rangle = \lim_{W \rightarrow \infty} \frac{1}{W} \int_{-W/2}^{W/2} \cdot dt \tag{3}$$

The spectral coherence function satisfies:

$$0 \leq |\rho_x^\alpha(f)| \leq 1 \tag{4}$$

$|\rho_x^\alpha(f)| = 1$  indicates that the two spectral lines of a random process  $x(t)$  are completely correlated at frequencies centered on spectral frequency,  $f$ , and separated by a cyclic frequency,  $\alpha$ ;  $|\rho_x^\alpha(f)| = 0$  suggests that the two spectral lines are completely uncorrelated. There must be a non-zero  $|\rho_x^\alpha(f)|$  when the random process,  $x(t)$ , is cyclostationary. In other words, the two discrete frequencies of the random process are correlated, and the distance between these two discrete frequencies must be equal to a certain cyclic frequency of the random process  $(f + \alpha/2) - (f - \alpha/2) = \alpha$ . Therefore, the cyclic frequency of the cyclostationary signal can be obtained by this method and then used for cyclic Wiener filtering.

### 2.2. Cyclic Wiener Filter

The cyclic Wiener filter is optimal in the sense of the least mean square, and it is proposed based on the spectral coherence theory of cyclostationary signals. The characteristic cyclic frequencies of cyclostationary signals are only required in advance. Then, the original signal traverses all characteristic cyclic frequencies to perform a set of frequency shifts. Finally, the adaptive filtering of the signal is realized through a filter bank.

If the target signal is cyclostationary, the adaptive filter for the stationary signal will no longer be applicable. Some researchers applied the basic ideas of Wiener filters, such as the Wiener–Hough equation, the steepest descent method, and the LMS (least mean square) algorithm, to cyclostationary signals and gradually formed the theory of cyclic Wiener filters that can be used for adaptive filtering of cyclostationary signals [27–30].

The so-called cyclic Wiener filter first shifts the frequency of the input signal,  $x(t)$ , with cyclostationarity:

$$x_\eta(t) = x(t) \cdot e^{j2\pi\eta t} \tag{5}$$

where  $\eta$  contains all the cyclic frequencies of  $x(t)$ . The shifted signal,  $x_\eta(t)$ , is selected as the new input signal. Then,  $x_\eta(t)$  is passed through the filter bank,  $h_\eta(t)$ , to obtain the respective output signal,  $y_\eta(t)$ , and  $y_\eta(t)$  is summed to acquire the total output signal,  $y(t)$ . The error function of  $e(t)$  is obtained by performing the difference operation with the expected output signals,  $d(t)$  and  $y(t)$ . The filter coefficients of each group are adaptively adjusted following  $e^2(t)$  to achieve optimal filtering. Figure 1a,b demonstrates the structural block diagrams of the adaptive filter and cyclic Wiener filter, respectively.

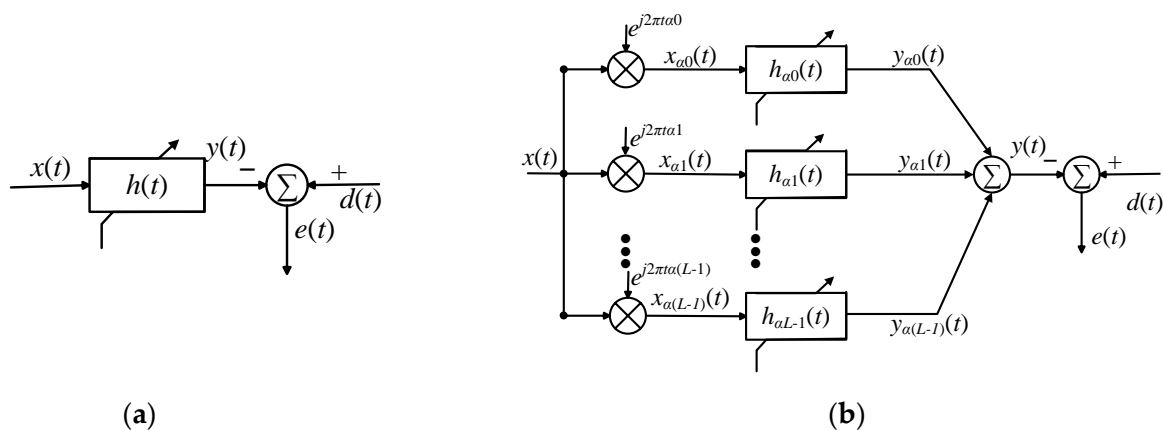


Figure 1. (a) Diagrams of the adaptive filter; (b) diagrams of the cyclic Wiener filter.

As observed in Figure 1, the cyclic Wiener filter is equivalent to the superposition of multiple adaptive filters.

However, the cyclic Wiener filter in practical applications is always implemented in a discrete form. Therefore, the relationship between the input and output of the cyclic Wiener filter can be obtained:

$$y(n) = \sum_{\eta} \sum_{m=0}^{M-1} w_{\eta,m} \cdot [x(n - m)e^{j2\pi \cdot \eta \cdot (n-m)}] \tag{6}$$

where  $\sum$  indicates the summation operator, and  $w_{\eta,0}, w_{\eta,1}, \dots$ , and  $w_{\eta,L-1}$  represent the weight coefficient of the filter,  $h_{\eta}(t)$ , corresponding to each cyclic frequency,  $\eta = \alpha_0, \alpha_1, \dots$ , and  $\alpha_{L-1}$ , respectively.

### 2.3. Cyclic Wiener Filter Adaptive Algorithm

The standard LMS adaptive iterative algorithm is used for cyclic Wiener filters. The iterative relationship of the LMS weight coefficients of the cyclic Wiener filter is:

$$\mathbf{w}(n + 1) = \mathbf{w}(n) + \mu[x_{\alpha_i}^*(n - k)e(n)] \tag{7}$$

where  $\mu$  denotes the step factor and is adopted to adjust the weight coefficient;  $w$  denotes a weight vector representing filter coefficients;  $x^*$  suggests taking the conjugate of  $x$ ;  $x_{\alpha_i}$  represents the new signal after the frequency shift,  $a$ , of  $\alpha_i$ . The iterative relationship of the weight coefficients is more intuitively demonstrated by expanding Equation (7) as:

$$\begin{bmatrix} \begin{bmatrix} w_{\alpha_0,0}(n + 1) \\ \vdots \\ w_{\alpha_0,M-1}(n + 1) \end{bmatrix} \\ \begin{bmatrix} w_{\alpha_1,0}(n + 1) \\ \vdots \\ w_{\alpha_1,M-1}(n + 1) \end{bmatrix} \\ \vdots \\ \begin{bmatrix} w_{\alpha_{L-1},0}(n + 1) \\ \vdots \\ w_{\alpha_{L-1},M-1}(n + 1) \end{bmatrix} \end{bmatrix} = \begin{bmatrix} \begin{bmatrix} w_{\alpha_0,0}(n) \\ \vdots \\ w_{\alpha_0,M-1}(n) \end{bmatrix} \\ \begin{bmatrix} w_{\alpha_1,0}(n) \\ \vdots \\ w_{\alpha_1,M-1}(n) \end{bmatrix} \\ \vdots \\ \begin{bmatrix} w_{\alpha_{L-1},0}(n) \\ \vdots \\ w_{\alpha_{L-1},M-1}(n) \end{bmatrix} \end{bmatrix} + \mu e(n) \begin{bmatrix} \begin{bmatrix} x_{\alpha_0}^*(n) \\ \vdots \\ x_{\alpha_0}^*(n - M + 1) \end{bmatrix} \\ \begin{bmatrix} x_{\alpha_1}^*(n) \\ \vdots \\ x_{\alpha_1}^*(n - M + 1) \end{bmatrix} \\ \vdots \\ \begin{bmatrix} x_{\alpha_{L-1}}^*(n) \\ \vdots \\ x_{\alpha_{L-1}}^*(n - M + 1) \end{bmatrix} \end{bmatrix} \tag{8}$$

### 3. Envelope Spectrum Analysis

Envelope spectrum analysis based on the Hilbert transform is a very effective method to extract characteristic frequencies, which have been widely used in bearing fault diagnosis. However, the characteristic frequency of bearing fault is often cyclostationary [31,32]. The Hilbert transform is the output response of  $s'(t)$ , obtained by passing a continuous-time signal  $s(t)$  through a linear system with an impulse response of  $1/\pi t$ . Make the original signal,  $x(t)$ , the real part of the envelope signal, the Hilbert transform,  $h(t)$ , of  $x(t)$  the imaginary part of the envelope signal, and then take the modulo to obtain the complex envelope signal of  $E(t)$ . Then, the envelope spectrum can be obtained by the Fourier transform of  $E(t)$ .

$h(t)$  is obtained by Hilbert transformation of signal  $x(t)$ :

$$h(t) = \frac{1}{\pi} \cdot \int_{-\infty}^{\infty} \frac{x(\tau)}{t - \tau} d\tau = \frac{1}{\pi t} * x(t) \tag{9}$$

where  $*$  indicates the convolution operator. The signals  $x(t)$  and  $h(t)$  form a new complex signal,  $z(t)$ , as the analytical signal:

$$z(t) = x(t) + jh(t) \tag{10}$$

The envelope of the complex signal  $z(t)$  is defined as:

$$E(t) = |z(t)| = |x(t) + jh(t)| = \sqrt{x^2(t) + h^2(t)} \tag{11}$$

The envelope spectrum is obtained by spectral analysis of the envelope signal,  $E(t)$ , which is sensitive to events related to impact force. The distribution of each frequency amplitude in the envelope spectrum is different from that in the spectrum. Specifically,

the amplitude of fault characteristic frequency in the spectrum diagram is small, and the amplitude of fault characteristic frequency in the envelope spectrum diagram is very high. This is easy to identify. Nevertheless, the fault characteristic frequency is generally consistent with the cyclic frequency. Therefore, the envelope spectrum eliminates unnecessary frequency interference and highlights the noise signal with cyclostationarity, compared to the spectrum analysis. Figure 2 exhibits the difference between the envelope spectrum and the spectrum of the Robinson R44 helicopter.

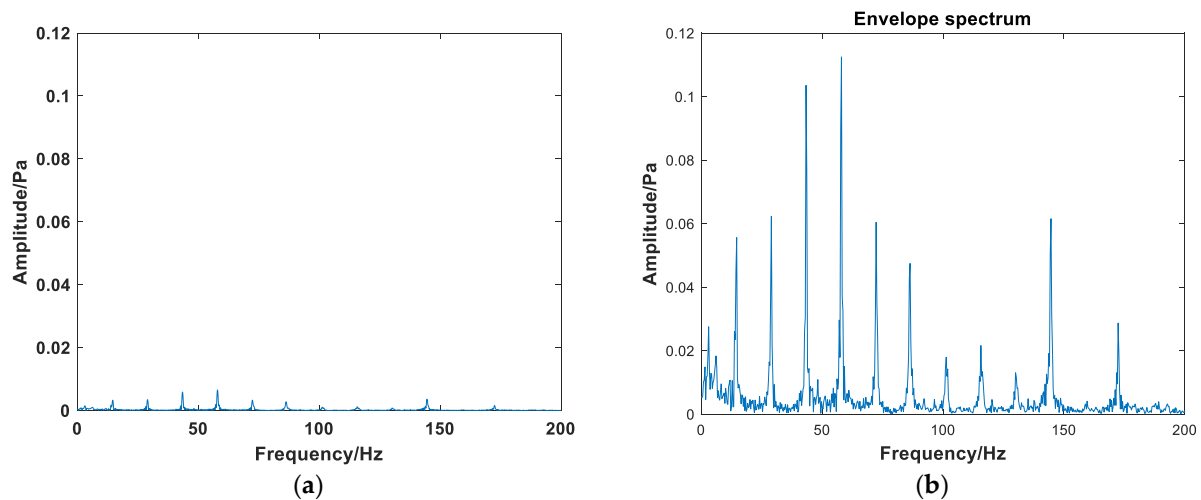


**Figure 2.** (a) Spectrum diagram of the Robinson R44 helicopter at 0.89 km; (b) envelope spectrum diagram of the Robinson R44 helicopter at 0.89 km.

Figure 2 reveals that the characteristics of rotor aerodynamic noise can be observed more clearly from the envelope spectrum.

#### 4. Experiment

A helicopter outfield flight test was conducted at an airport in Beichuan to verify the effectiveness of the proposed method for rotor aerodynamic noise signal enhancement. The flight data of the Robinson R44 helicopter was obtained. Robinson R44 helicopter is displayed in Figure 3.



**Figure 3.** Robinson R44 helicopter.

There are many devices in the whole helicopter acoustic target experiment. Table 1 gives the names, quantities, and uses of most of these devices. The sensitivity of the microphone is about 4 mV/Pa; the RTK (real-time kinematic) of the handheld GPS is 2.5 cm + 1 ppm, and its tracking sensitivity is 158 dBm; the RTK of the differential positioning device is 1.5 cm + 1 ppm; the heading accuracy is less than 0.2°. As we all know, the

most important device for collecting acoustic signals is the microphone, which is a sensor that converts acoustic signals into electrical signals. Therefore, it is necessary to analyze the uncertainty of the microphone, which is  $\pm 0.06$  dB at a 250 Hz acoustic input signal. The experimental process is presented in Figure 4.

**Table 1.** Experimental devices.

Measurement Equipment	Amount	Purpose
Data acquisition host computer	1	Running the helicopter acoustic detection data acquisition and processing software.
Controller/power box	1	Data acquisition equipment control and power supply.
Data acquisition equipment	9	Controlling microphones to capture noise/data relay.
Microphone array frame	9	Supporting and mounting the microphones.
Array transmission cable	9	Equipment power supply and signal transmission.
Microphone	9 × 15	Acquiring noise signals.
Dedicated mobile hard disk	1	Data storage.
Handheld GPS device	1	Recording helicopter position.
Differential positioning device	1	Recording the position of the microphone array.



(a)



(b)

**Figure 4.** Helicopter acoustic target detection experiment. (a) An array frame; (b) Robinson R44 helicopter flight experiment site.

The SNR is high when the helicopter is close to the microphone. However, the SNR gradually decreases with the increase in the distance between the helicopter and the microphone, due to the attenuation of the helicopter acoustic signal when it propagates in the air. During the field flight test, the helicopter first started from a short distance, gradually flew farther, and then flew back. Additionally, the distance between the Robinson R44 helicopter and the microphone is provided in Figure 5.

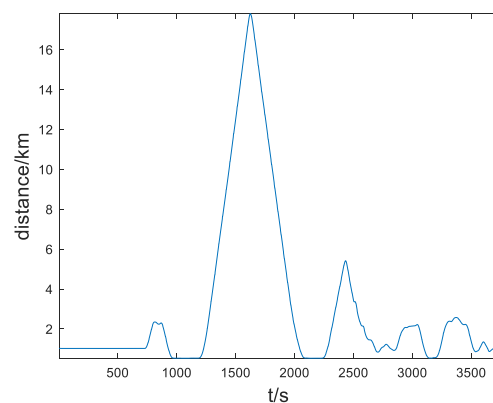


**Figure 5.** Robinson R44 helicopter distance from the microphone.

#### 4.1. Cyclic Frequency Detection

Antoni proposed a fast computation of the spectral correlation [33]. Therefore, the cyclic spectral correlation density function,  $S_x^\alpha(f)$ , and spectral coherence function,  $\rho_x^\alpha(f)$ , of the target signal were obtained quickly. The detection method of the cyclic frequency was derived from the detection function:

$$T(\alpha) = \int_0^{f_s/2} |\rho_x^\alpha(f)|^2 df \quad (12)$$

where  $\rho_x^\alpha(f)$  indicates the cyclic spectral coherence function of the target signal, obtained by Equation (1), and  $f_s$  indicates sampling frequency, which is defined as 2500 Hz in the experiment.

The time period from far to near (18 km to 0 km) was selected for analysis. The cyclic frequencies were first obtained at a close distance and then gradually detected farther away, until the limit distance where the cyclic frequency can be detected was found.

First, the cyclic frequency detection was performed at 0.89 km. Figure 6 exhibits the cyclic spectrum coherence function graph and the cyclic frequency detection result. The abscissas of these peaks in Figure 6b denote the cyclic frequencies. Liang Yu concluded that rotor aerodynamic noise is characterized by the fundamental cyclic frequency and its multiplier [22,23]. Thus, the cyclic frequency detection result in Figure 6 was correct.

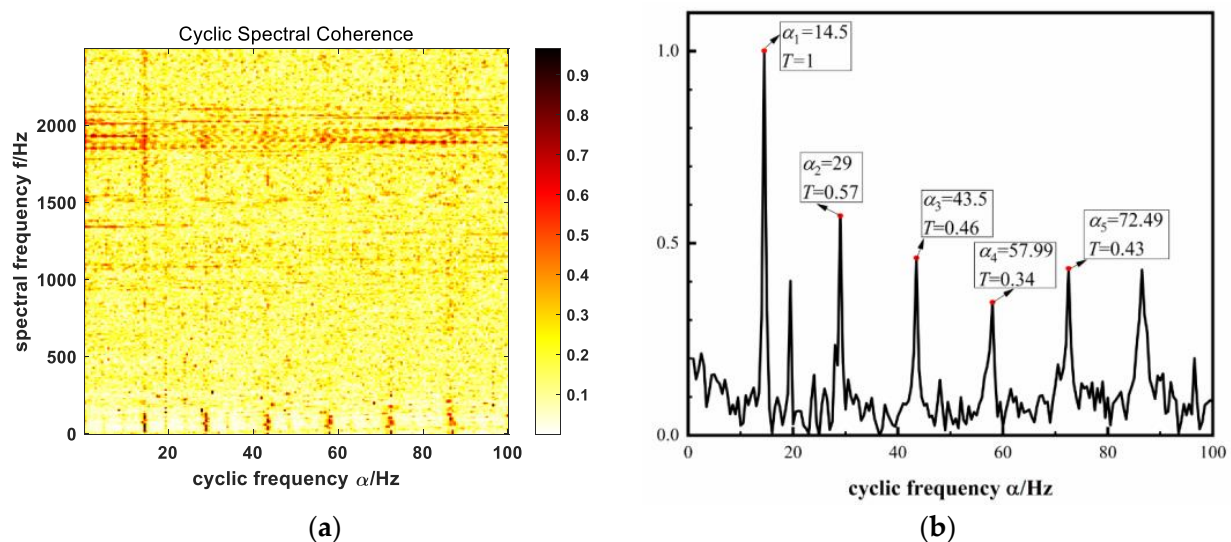


**Figure 6.** (a) The cyclic spectrum coherence function graph of the Robinson R44 helicopter at 0.89 km; (b) the cyclic frequency detection results of the Robinson R44 helicopter at 0.89 km.

Then, the cyclic frequency detection was conducted at 1.548 km. Figure 7 presents the cyclic spectrum coherence function graph and the cyclic frequency detection result of the Robinson R44 helicopter at this distance.

The cyclic frequency detection was also achieved at 3.568 km, and the results are demonstrated in Figure 8.

After a lot of tests, the limit distance was revealed to be 4.114 km. Figure 9 illustrates the spectral coherence function and cyclic frequency at this distance. It was suggested that the multiple relationships of the cyclic frequency were not significant.

Finally, the detection results of cyclic frequency at 17.75 km were obtained, as exhibited in Figure 10. The cyclic frequency of the Robinson R44 helicopter is completely invisible from this graph.

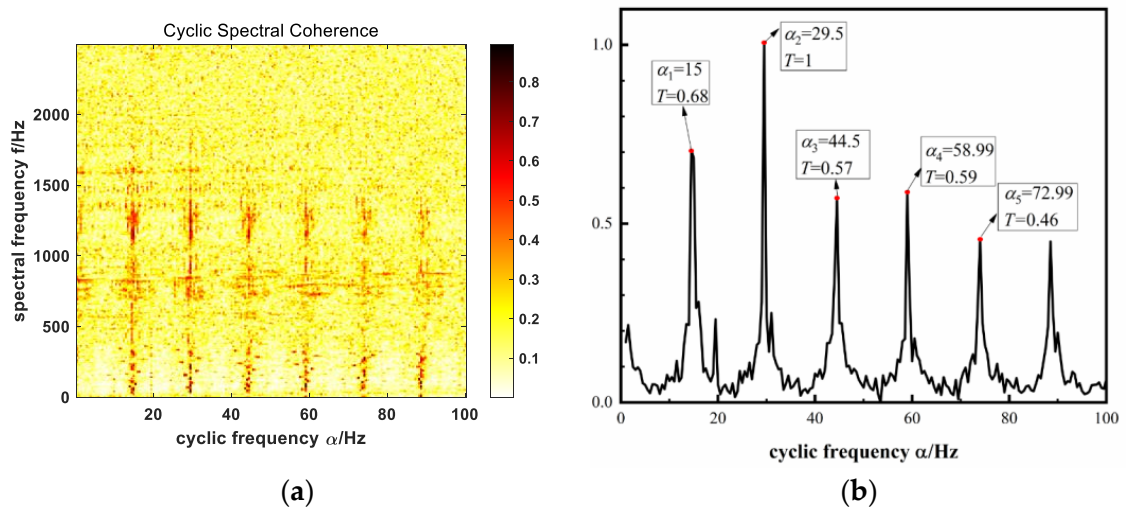


**Figure 7.** (a) The cyclic spectrum coherence function graph of the Robinson R44 helicopter at 1.548 km; (b) the cyclic frequency detection results of the Robinson R44 helicopter at 1.548 km.

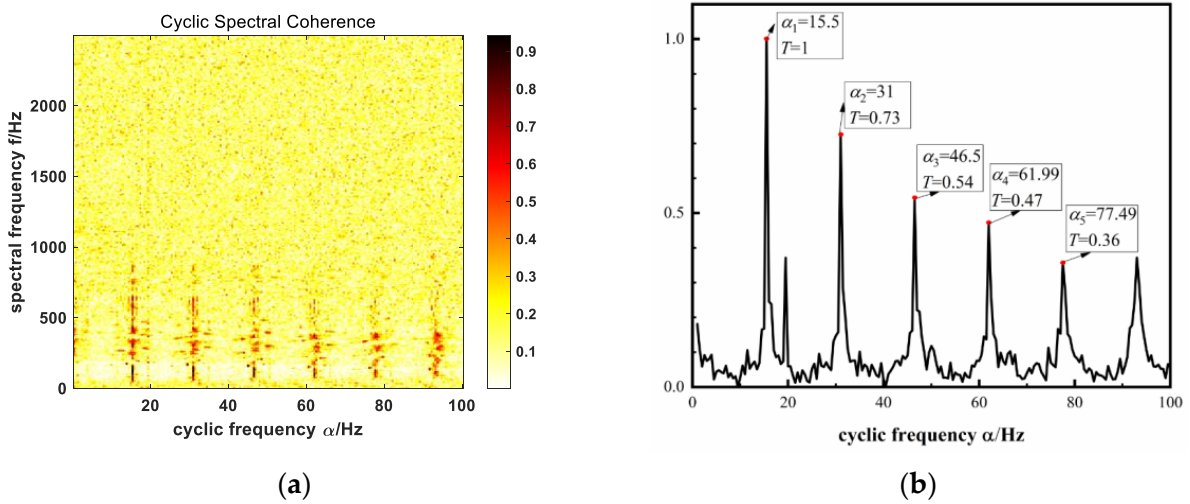


**Figure 8.** (a) The cyclic spectrum coherence function graph of the Robinson R44 helicopter at 3.568 km; (b) the cyclic frequency detection results of the Robinson R44 helicopter at 3.568 km.

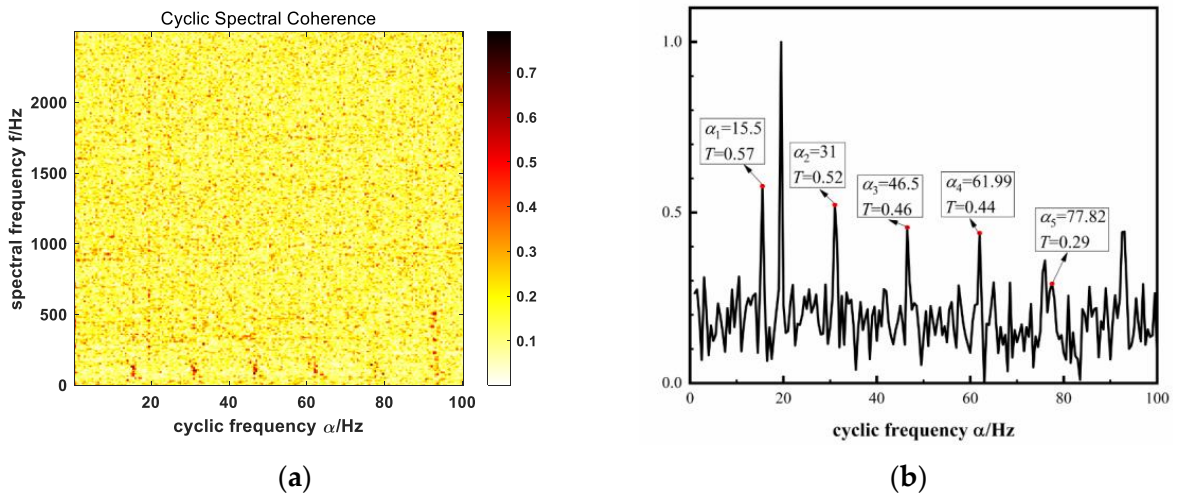


**Figure 9.** (a) The cyclic spectrum coherence function graph of the Robinson R44 helicopter at 4.114 km; (b) the cyclic frequency detection results of the Robinson R44 helicopter at 4.114 km.

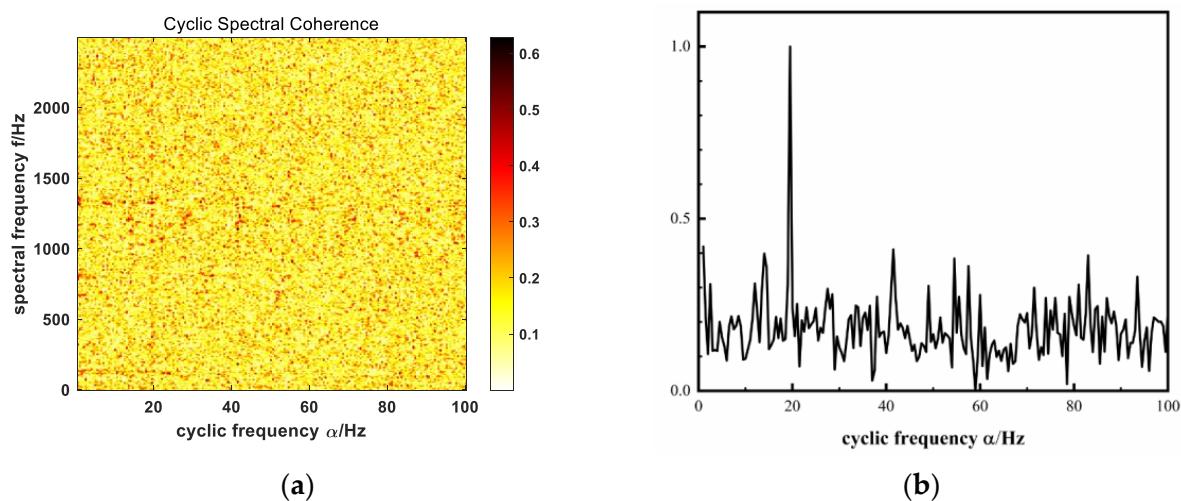


**Figure 10.** (a) The cyclic spectrum coherence function graph of the Robinson R44 helicopter at 17.75 km; (b) the cyclic frequency detection results of the Robinson R44 helicopter at 17.75 km.

As suggested in Figures 6–10, the characteristic of the cyclic frequency gradually changed from clear to fuzzy. This can be explained because with the increase in the distance, there was more and more attenuation as it traveled through the air, resulting in a lower and lower SNR. The comparison of Figures 6–8 demonstrated that the cyclic frequency deviated when the cyclic frequency was detected at different distances. This was induced by the phenomenon of a Doppler frequency shift. The result of cyclic frequency detection was gradually blurred with the increase in the distance. In Figure 10, the cyclic frequency was completely invisible at 17.75 km. This result was consistent with the result of envelope spectrum analysis.

#### 4.2. Filtering

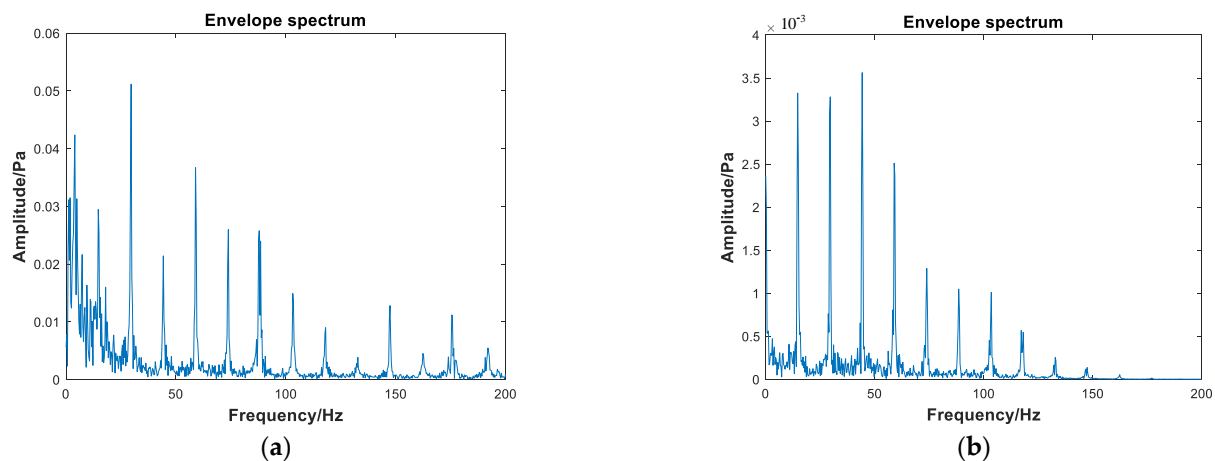
The cyclic frequencies of rotor aerodynamic noise at different distances were obtained, and then the frequency shift was carried out according to the cyclic frequency detection method in Section 4.1. The detection results of several groups of cyclic frequencies are given in Table 2, which are used in the following cyclic Wiener filter.

**Table 2.** Detection results of cyclic frequencies at different distances.

Distance/km	Cyclic Frequency/Hz
0.89	$\eta = [14.5 \ 29.0 \ 43.5 \ 57.99 \ 72.49]$
1.548	$\eta = [15.0 \ 29.5 \ 44.5 \ 58.99 \ 73.99]$
3.568	$\eta = [15.5 \ 31.0 \ 46.5 \ 61.99 \ 77.49]$
4.114	$\eta = [15.5 \ 31.0 \ 46.5 \ 61.99 \ 77.49]$

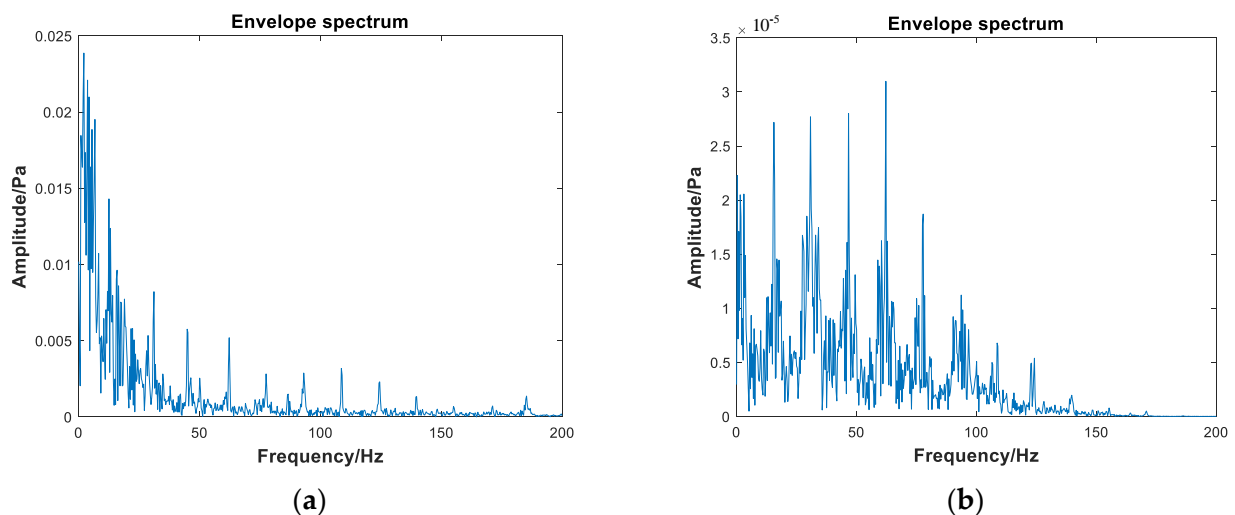
Since the aerodynamic noise of the main rotor of the helicopter is mainly in low frequency, it should be band-pass filtered first to filter out some irrelevant background noise, followed by cyclic Wiener filtering. The cyclic frequency,  $\eta$ , was inputted for frequency shifting, and the signal after the band-pass filter was taken as the expected response, so as to filter out the background noise adaptively. The filtering effects of the three distance points are exhibited in Figures 7, 9 and 10, respectively.

Figure 11 displays the envelope spectrum of the Robinson R44 helicopter before and after filtering at 1.548 km. Compared with Figures 11a and 11b, there was less attenuation when propagating in the air owing to the short distance, contributing to a high SNR. Therefore, the characteristics before filtering were significant. Moreover, the characteristics of target information can be observed more clearly through the envelope spectrum after cyclic Wiener filtering.



**Figure 11.** (a) Envelope spectrum of the Robinson R44 helicopter before filtering at 1.548 km; (b) Envelope spectrum of the Robinson R44 helicopter after filtering at 1.548 km.

At the distance of 4.114 km, the cyclic frequency obtained from Table 2 is  $\eta = [15.5 \ 31 \ 46.5 \ 61.99 \ 77.49]$ , and it is applied to the frequency shift of cyclic Wiener filtering. The filtering result is shown in Figure 12.



**Figure 12.** (a) Envelope spectrum of the Robinson R44 helicopter before filtering at 4.114 km; (b) Envelope spectrum of the Robinson R44 helicopter after filtering at 4.114 km.

The filtering effect of the Robinson R44 helicopter at 4.114 km is presented in Figure 12. As revealed by comparing Figures 12a and 12b, there was more attenuation when propagating in the air because the position here is far away, leading to a low SNR. Therefore, the characteristics before filtering are not significant, and the characteristics of helicopter rotor aerodynamic noise can be observed through the envelope spectrum after cyclic Wiener filtering.

After cyclic Wiener filtering is performed point by point, it was discovered that the limit distance of the rotor aerodynamic noise characteristic observed through the envelope spectrum after filtering was 17.75 km, in line with Figure 10. At 17.75 km, the cyclic frequency cannot be detected at all. However, in comparison with Figures 6–8, it can be seen that the farther the distance is, the higher the cyclic frequency is, relatively. Therefore, when inputting the cyclic frequency to conduct a frequency shift over a long distance, the cyclic frequency needs to be increased properly. After multiple attempts, the cyclic frequency,  $\eta = [15.75 \ 31.13 \ 44.98 \ 62.19 \ 77.82]$ , was finally selected to conduct a frequency shift. The envelope spectrum before filtering with a distance of 17.75 km is provided

in Figure 13a. The characteristics of the target information were not observed through this envelope spectrum. The filtered envelope spectrum is exhibited in Figure 13b. The characteristics of the target information were observed through several spectral lines in the figure.

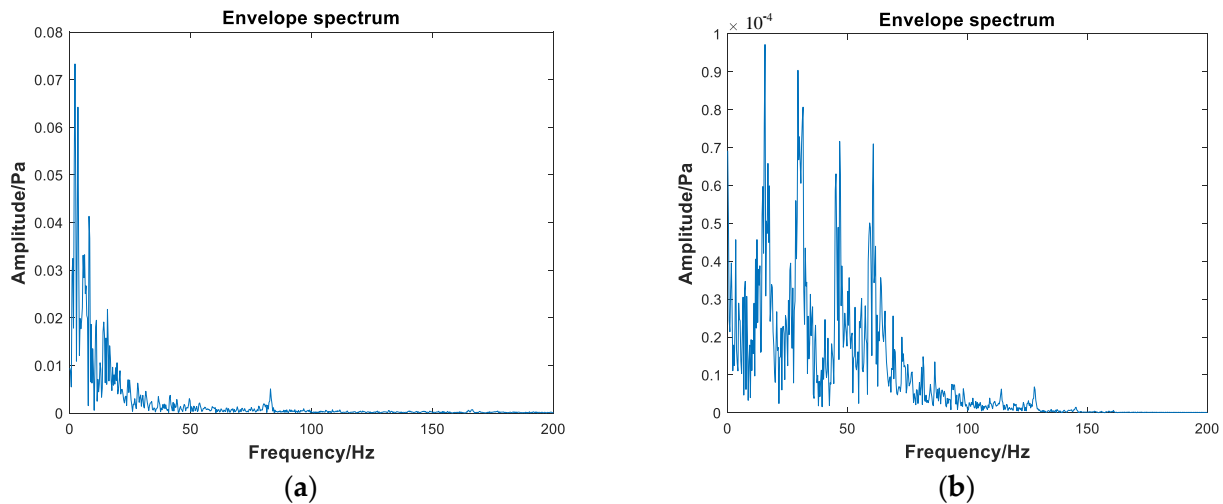


**Figure 13.** (a) Envelope spectrum of the Robinson R44 helicopter before filtering at 17.75 km; (b) Envelope spectrum of the Robinson R44 helicopter after filtering at 17.75 km.

#### 4.3. Helicopter Long-Distance Detection

The rotor aerodynamic noise will exhibit the harmonic characteristics of the blade passing frequency and its higher-order harmonics in the frequency domain when the helicopter is in operation. Therefore, the detection algorithm was constructed following the envelope spectrum and combined with the harmonic characteristics of the rotor aerodynamic noise to display the detection results intuitively, so as to avoid looking at the envelope spectrum whenever viewing the filtering effect. Next, the spectral peaks were discovered by constructing the spectral peak search function, and whether the helicopter signal was detected was judged according to the constructed, complete detection function. The flow chart of the detection algorithm is provided in Figure 14.

The part of the Robinson R44 helicopter flying close from a long distance was intercepted, and the detection results were obtained based on the distance, as illustrated in Figure 15. Specifically, one indicates that a helicopter signal was detected, and zero indicates that no helicopter signal was detected. Moreover, the detection rate was calculated every 100 s, allowing it to more clearly judge whether the helicopter signal was effectively detected.

Before filtering, in Figure 15, the detection rate prior to  $t = 1947$  s (corresponding to a distance of 4.114 km) was relatively low, indicating that the helicopter signal cannot be effectively detected. However, the detection rate after filtering was considerable, reflecting that the helicopter signal can be effectively detected. This further confirmed that the cyclic Wiener filter exerted a good enhancement effect on the helicopter rotor aerodynamic noise signal.

During the field flight experiment, the background noise signal was collected deliberately, and the correctness of the detection code was verified by the background noise signal. The detection rate of the background noise signal is also called the false alarm rate. The false alarm rate of the background noise signal is presented in Figure 16.

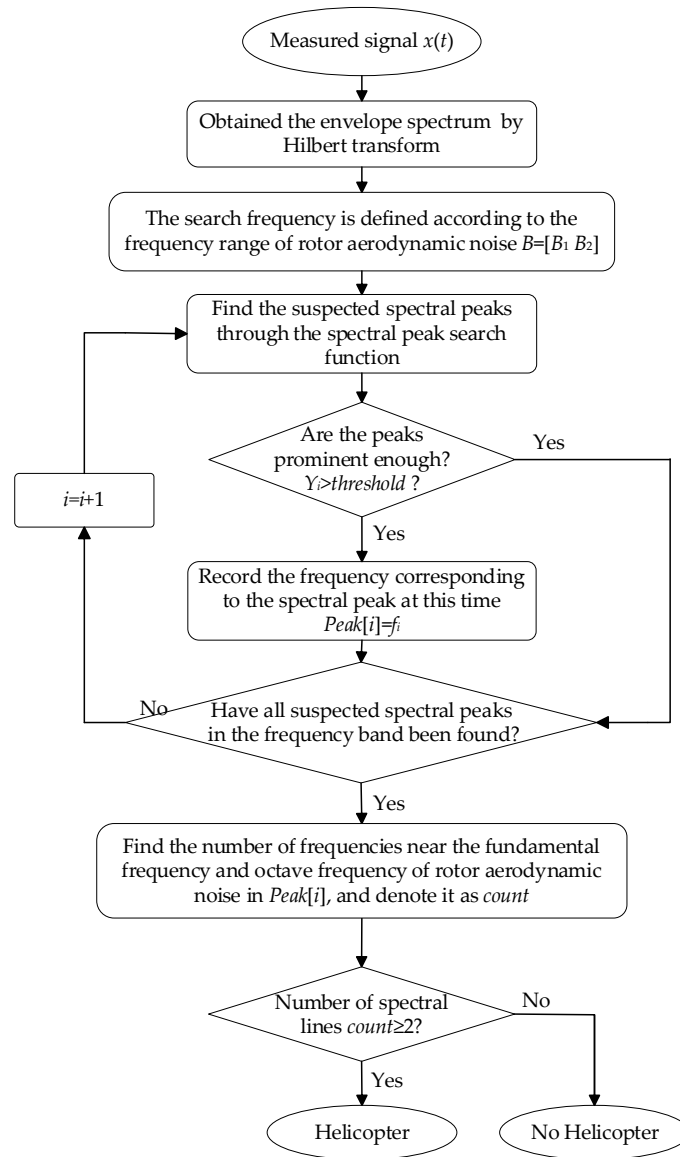


Figure 14. Flow chart of detection algorithm of helicopter.

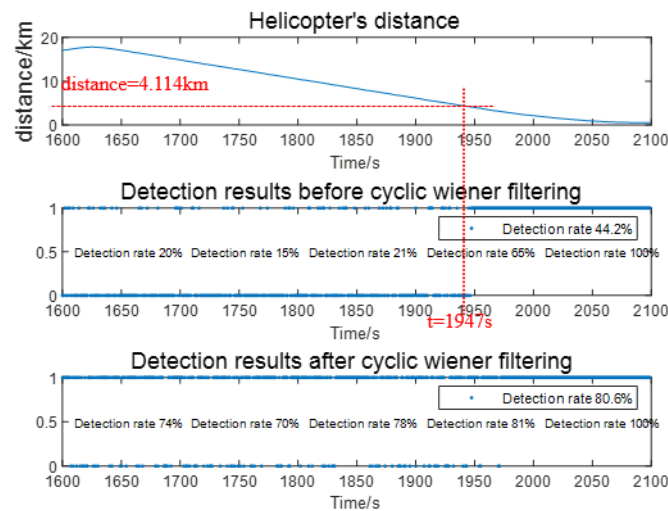
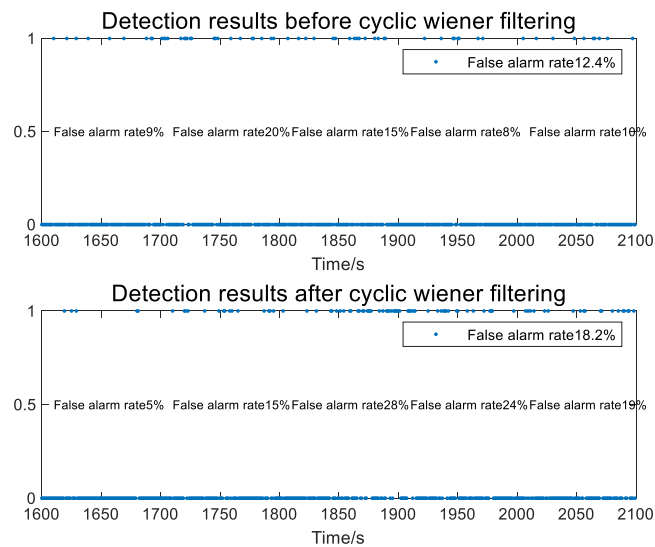


Figure 15. Helicopter long-distance detection results.



**Figure 16.** False alarm rate of background noise signal.

As demonstrated in Figure 16, the false alarm rate with the background noise as the input signal for helicopter detection was extremely low, suggesting that the detection algorithm did not judge the background noise signal as the helicopter signal, consistent with the established fact. Figures 15 and 16 revealed that the filtered detection rate for the helicopter noise signal varied from low to high. Meanwhile, the false alarm rate before and after filtering for background noise signals was relatively low. This implied that the detection algorithm effectively distinguished the helicopter signal from the background noise signal, fully verifying the correctness of the detection algorithm.

## 5. Conclusions

In this paper, a cyclic Wiener filter was proposed for its signal enhancement according to the cyclostationary characteristics of rotor aerodynamic noise. Additionally, how to achieve filtering by cyclic Wiener filter was theoretically investigated. Furthermore, the necessity of envelope spectrum analysis was analyzed. According to the harmonic characteristics of rotor aerodynamic noise, a detection function was constructed to realize helicopter detection. Based on the data of the helicopter acoustic target detection experiment, the main conclusions can be summarized as follows:

1. The cyclic frequencies were first obtained at a close distance and then gradually detected farther away, until the limit distance where the cyclic frequency can be detected was found. This limit distance was revealed to be 4.114 km. Meanwhile, when comparing the cyclic frequencies at different distances, it is found that due to the influence of the Doppler frequency shift, the cyclic frequencies will be higher in the case of long distances than in the case of short distances.
2. The collected noise signal was subjected to cyclic Wiener filtering, and its filtering effect is analyzed combined with envelope spectrum. When cyclic Wiener filtering is performed at a close range, the frequency shift can be performed according to the detected cyclic frequency. However, For the case that the distance exceeds the limit distance of 4.114 km, it is necessary to appropriately increase the cyclic frequencies for correction, because in this case, the rotor aerodynamic noise with cyclostationarity has been submerged by the strong background noise, so the cyclic frequency detection is unable to detect its cyclic frequencies normally. Before filtering, the limit distance of the features of rotor aerodynamic noise through envelope spectrum analysis was 4.114 km, which is consistent with the limit distance at which the cyclic frequencies can be detected. The detection distance after cyclic Wiener filtering reaches 17.75 km, which is greatly improved compared to before filtering.

3. According to the helicopter detection algorithm constructed in this paper, the collected helicopter noise signals are used for helicopter detection. The comparison before and after the cyclic Wiener filtering shows that the cyclic Wiener filter can effectively improve the detection rate of helicopters. For the time period when the helicopter flew from 18 km to 0 km, the detection rate before filtering was 44.2%, and the detection rate after filtering was 80.6%. Moreover, the cyclic Wiener filter can effectively improve the detection distance of the helicopter. In order to verify the correctness of the detection code, the background noise signal was collected separately during the experiment. The detection function is used to detect this background noise signal. The false alarm rate before and after cyclic Wiener filtering is very low, which is 12.4% before filtering and only 18.2% after filtering, which is consistent with the established fact.

Due to the cyclostationarity of helicopter rotor aerodynamic noise, the application of other cyclostationarity analysis methods to helicopter rotor aerodynamic noise can certainly be further studied. In addition, regarding the use of helicopter acoustic signals to detect helicopters, the rest of the acoustic signal processing methods will also be further explored.

**Author Contributions:** Conceptualization, C.W. (Chengfeng Wu) and C.W. (Chunhua Wei); data curation, C.W. (Chengfeng Wu) and C.W. (Chunhua Wei); formal analysis, C.W. (Chengfeng Wu); funding acquisition, C.W. (Chunhua Wei); investigation, C.W. (Chengfeng Wu) and C.W. (Chunhua Wei); methodology, C.W. (Chunhua Wei); project administration, C.W. (Chunhua Wei) and Y.W.; resources, C.W. (Chunhua Wei) and Y.W.; software, C.W. (Chengfeng Wu); supervision, C.W. (Chunhua Wei) and Y.W.; validation, C.W. (Chengfeng Wu), C.W. (Chunhua Wei), and Y.W.; visualization, C.W. (Chengfeng Wu); writing—original draft, C.W. (Chengfeng Wu) and C.W. (Chunhua Wei); writing—review and editing, C.W. (Chengfeng Wu), Y.W. and Y.G. All authors have read and agreed to the published version of the manuscript.

**Funding:** This research was funded by the National Natural Science Foundation of China under grant number 51275523, the State Key Laboratory of Aerodynamics Research Fund under grant number SKLA2019040302.

**Institutional Review Board Statement:** Not applicable.

**Informed Consent Statement:** Not applicable.

**Data Availability Statement:** Not applicable.

**Acknowledgments:** The authors extend their appreciation to Southwest University of Science and Technology, and State Key Laboratory of Aerodynamics, China Aerodynamics Research and Development Center for their technical support.

**Conflicts of Interest:** The authors declare no conflict of interest.

## References

1. Erickson, L.C.; Newman, R.S. Influences of background noise on infants and children. *Curr. Dir. Psychol. Sci.* **2017**, *26*, 451–457. [[CrossRef](#)] [[PubMed](#)]
2. Minichilli, F.; Gorini, F.; Ascari, E.; Bianchi, F.; Coi, A.; Fredianelli, L.; Licitra, G.; Manzoli, F.; Mezzasalma, L.; Cori, L. Annoyance Judgment and Measurements of Environmental Noise: A Focus on Italian Secondary Schools. *Environ. Res. Public Health* **2018**, *15*, 208. [[CrossRef](#)] [[PubMed](#)]
3. Rossi, L.; Prato, A.; Lesina, L.; Schiavi, A. Effects of low-frequency noise on human cognitive performances in laboratory. *Build. Acoust.* **2018**, *25*, 17–33. [[CrossRef](#)]
4. Petri, D.; Licitra, G.; Vigotti, M.A.; Fredianelli, L. Effects of Exposure to Road, Railway, Airport and Recreational Noise on Blood Pressure and Hypertension. *Environ. Res. Public Health* **2021**, *18*, 9145. [[CrossRef](#)]
5. Vukic, L.; Mihanovic, V.; Fredianelli, L.; Plazibat, V. Seafarers' Perception and Attitudes towards Noise Emission on Board Ships. *Environ. Res. Public Health* **2021**, *18*, 6671. [[CrossRef](#)]
6. Petrescu, R.V.; Aversa, R.; Akash, B.; Corchado, J.; Berto, F.; Apicella, A.; Petrescu, F.I. About Helicopters. *J. Aircr. Spacecr. Technol.* **2017**, *1*, 204–223. [[CrossRef](#)]
7. Shi, Y.J.; Li, T.; He, X.; Dong, L.H.; Xu, G.H. Helicopter Rotor Thickness Noise Control Using Unsteady Force Excitation. *Appl. Sci.* **2019**, *9*, 1351. [[CrossRef](#)]
8. George, A.R. Helicopter noise: State-of-the-art. *J. Aircr.* **1978**, *15*, 707–715. [[CrossRef](#)]

9. Schmitz, F.H. The challenges and possibilities of a truly quiet helicopter 29th Alexander a Nikolsky Honorary Lecture. *J. Am. Helicopter Soc.* **2016**, *61*, 1–33. [[CrossRef](#)]
10. Brentner, K.S.; Farassat, F. Modeling aerodynamically generated sound of helicopter rotors. *Prog. Aerosp. Sci.* **2003**, *39*, 83–120. [[CrossRef](#)]
11. Yin, J.; Ahmed, S. Aerodynamics and Aeroacoustics of Helicopter Main-Rotor/Tail-Rotor Interaction. In Proceedings of the 5th AIAA/CEAS Aeroacoustics Conference and Exhibit, Bellevue, WA, USA, 10–12 May 1999.
12. Brentner, K. An efficient and robust method for predicting helicopter high-speed impulsive noise. *J. Sound Vib.* **1997**, *203*, 87–100. [[CrossRef](#)]
13. Wohlbrandt, A.M.; Guerin, S.; Ewert, R. Simultaneous Computation of Surface and Volume Sources for Fan Broadband Noise with the Random-Particle-Mesh Method. In Proceedings of the 19th AIAA/CEAS Aeroacoustics Conference, Berlin, Germany, 27–29 May 2013.
14. Antoni, J.; Bonnardot, F.; Raad, A.; Badaoui, M.E. Cyclostationary modelling of rotating machine vibration signals. *Mech. Syst. Signal Process.* **2004**, *18*, 1285–1314. [[CrossRef](#)]
15. Antoni, J. Cyclic spectral analysis in practice. *Mech. Syst. Signal Process.* **2007**, *21*, 597–630. [[CrossRef](#)]
16. Antoni, J. Cyclic spectral analysis of rolling-element bearing signals: Facts and fictions. *J. Sound Vib.* **2007**, *304*, 497–529. [[CrossRef](#)]
17. Antoni, J. Cyclostationarity by examples. *Mech. Syst. Signal Process.* **2009**, *23*, 987–1036. [[CrossRef](#)]
18. Timofey, S.; Oksana, G.; Yury, K. Cyclostationary Approach to the Analysis of the Power in Electric Circuits under Periodic Excitations. *Appl. Sci.* **2021**, *11*, 9711. [[CrossRef](#)]
19. Miao, H.; Zhang, F.; Tao, R. New statistics of the second-order chirp cyclostationary signals: Definitions, properties and applications. *IEEE Trans. Signal Process.* **2019**, *67*, 5543–5557. [[CrossRef](#)]
20. Miao, H.; Zhang, F.; Tao, R. A general fraction-of-time probability framework for chirp cyclostationary signals. *Signal Process.* **2021**, *179*, 107820. [[CrossRef](#)]
21. Miao, H.; Zhang, F.; Tao, R. Novel second-order statistics of the chirp cyclostationary signals. *IEEE Signal Process. Lett.* **2020**, *27*, 910–914. [[CrossRef](#)]
22. Yu, L.; Wu, H.; Antoni, J.; Jiang, W. Extraction and imaging of aerodynamically generated sound field of rotor blades in the wind tunnel test. *Mech. Syst. Signal Process.* **2019**, *116*, 1017–1028. [[CrossRef](#)]
23. Yu, L.; Yu, L.; Wang, J.; Wang, R.; Chen, Z. Cyclostationary modeling for the aerodynamically generated sound of helicopter rotors. *Mech. Syst. Signal Process.* **2022**, *168*, 108680. [[CrossRef](#)]
24. Boustany, R.; Antoni, J. Blind Extraction of a Cyclostationary Signal Using Reduced-Rank Cyclic Regression—A Unifying Approach. *Mech. Syst. Signal Process.* **2008**, *22*, 520–541. [[CrossRef](#)]
25. Antoni, J.; Leclère, Q.; Dinselmeyer, A.; Julliard, E.; Bouley, S.; Picard, C.; Sijtsma, P. Stand-Alone Extraction of Cyclostationary Broadband Components from Aeroacoustic Signals. *AIAA J.* **2022**, *60*, 1817–1832. [[CrossRef](#)]
26. Monakov, A.A. Radar Detection and Recognition of a Hovering Helicopter. In Proceedings of the 2021 Wave Electronics and its Application in Information and Telecommunication Systems (WECONF), St. Petersburg, Russia, 31 May–4 June 2021.
27. Gardner, W.A.; Brown, W.A. Frequency-shift filtering theory for adaptive co-channel interference removal. In Proceedings of the Twenty-Third annual Asilomar Conference on Signals, Systems, and Computers, Pacific Grove, CA, USA, 1 October 1989.
28. Dong, G.M.; Chen, J.; Ming, Y. Feature Extraction Based on Cyclic Adaptive Filter for Gearbox Fault Diagnosis. *Lect. Notes Control Inf. Sci.* **2015**, *20*, 175–187. [[CrossRef](#)]
29. Yu, L.; Antoni, J.; Wu, H.J.; Jiang, W.K. Reconstruction of cyclostationary sound source based on a back-propagating cyclic wiener filter. *J. Sound Vib.* **2018**, *442*, 787–799. [[CrossRef](#)]
30. Yu, D.J.; Cheng, J.S.; Yang, Y. Application of EMD method and Hilbert spectrum to the fault diagnosis of roller bearings. *Mech. Syst. Signal Process.* **2005**, *19*, 259–270. [[CrossRef](#)]
31. Sheen, Y.T. A complex filter for vibration signal demodulation in bearing defect diagnosis. *J. Sound Vib.* **2004**, *276*, 105–119. [[CrossRef](#)]
32. Wang, R.; Zhang, C.Y.; Yu, L.; Fang, H.T.; Hu, X. Rolling Bearing Weak Fault Feature Extraction under Variable Speed Conditions via Joint Sparsity and Low-Rankness in the Cyclic Order-Frequency Domain. *Appl. Sci.* **2022**, *12*, 2449. [[CrossRef](#)]
33. Antoni, J.; Xin, G.; Hamzaoui, N. Fast computation of the spectral correlation. *Mech. Syst. Signal Process.* **2017**, *92*, 248–277. [[CrossRef](#)]